

Modeling soil thermal and hydrological dynamics and changes of growing season in Alaskan terrestrial ecosystems

Jinyun Tang · Qianlai Zhuang

Received: 30 January 2009 / Accepted: 5 October 2010
© Springer Science+Business Media B.V. 2010

Abstract Abundant evidence indicates the growing season has been changed in the Alaskan terrestrial ecosystems in the last century as climate warms. Reasonable simulations of growing season length, onset, and ending are critical to a better understanding of carbon dynamics in these ecosystems. Recent ecosystem modeling studies have been slow to consider the interactive effects of soil thermal and hydrological dynamics on growing season changes in northern high latitudes. Here, we develop a coupled framework to model these dynamics and their effects on plant growing season at a daily time step. In this framework, we (1) incorporate a daily time step snow model into our existing hydrological and soil thermal models and (2) explicitly model the moisture effects on soil thermal conductivity and heat capacity and the effects of active layer depth and soil temperature on hydrological dynamics. The new framework is able to well simulate snow depth and soil temperature profiles for both boreal forest and tundra ecosystems at the site level. The framework is then applied to Alaskan boreal forest and tundra ecosystems for the period 1923–2099. Regional simulations show that (1) for the historical period, the growing season length, onset, and ending, estimated based on the mean soil temperature of the top 20 cm soils, and the annual cycle of snow dynamics, agree well with estimates based on satellite data and other approaches and (2) for the projected period, the plant growing season length shows an increasing trend in both tundra and boreal forest ecosystems. In response to the projected warming, by year 2099, (1) the snow-free days will be increased by 41.0 and 27.5 days, respectively, in boreal forest and tundra ecosystems and (2) the growing season lengths will be more than 28 and 13 days longer in boreal forest and tundra ecosystems, respectively, compared to 2010.

J. Tang (✉) · Q. Zhuang
Purdue Climate Change Research Center, Department of Earth and Atmospheric Sciences,
Purdue University, West Lafayette, IN, USA
e-mail: tang16@purdue.edu

Q. Zhuang
Department of Agronomy, Purdue University, West Lafayette, IN, USA

Comparing two sets of simulations with and without considering feedbacks between soil thermal and hydrological dynamics, our analyses suggest coupling hydrological and soil thermal dynamics in Alaskan terrestrial ecosystems is important to model ecosystem dynamics, including growing season changes.

1 Introduction

The last century has seen an increase in surface air temperature in many places over the globe. Analyses based on observational records show that such an increase is as much as 0.6°C since 1861 globally (Jones et al. 1999), while the Arctic region has experienced the greatest warming in the most recent decades (Serreze et al. 2000). The climatic change in the Arctic has led to greening in arctic ecosystems since the 1980s (Myneni et al. 1997; Jia et al. 2003; Goetz et al. 2005; Verbyla 2008). The growing season change has profound implications to carbon dynamics. On the one hand, abundant evidence suggests that the growing season in northern high latitudes has been affected by changes of soil thermal regime (Kimball et al. 2004). And greening in a warmer climate increases the photosynthetic activity and enhances carbon uptake in the region (Slayback et al. 2003; Kimball et al. 2007). On the other hand, a warmer climate stimulates permafrost thawing, causing more carbon released to the atmosphere (Zimov et al. 2006), thus a positive feedback to the climate system (Hansen et al. 2005). To date, while modeling efforts have been focused on modeling the fate of soil carbon (e.g. Zhuang et al. 2003; Euskirchen et al. 2006; Balshi et al. 2007), the growing season changes have not been well modeled at large scales. Since, by definition, the growing season indicates the length of time that allows the plant to assimilate carbon from atmosphere, the modeling of growing season change is an important step towards a better understanding of future climate change on carbon dynamics. Here we investigate how growing season in Alaska has changed and will change from 1923 to 2099 by simulating the changes of soil thermal regimes at a daily time step.

To more reasonably model soil thermal dynamics at a daily time step, we further develop an existing framework of soil thermal and hydrological dynamics (Zhuang et al. 2001, 2002, 2003, 2004). The existing framework was shown to reasonably simulate soil thermal regimes at site and regional scales and at a monthly time step (Zhuang et al. 2002, 2004; Euskirchen et al. 2006; Balshi et al. 2007). However, the existing framework has several limitations. (1) It has not explicitly considered the feedbacks between dynamics of soil thermal regime and hydrological conditions, i.e. the soil moisture of each soil layers were prescribed. The intimate coupling between soil thermal and hydrological dynamics is of particular importance in the cold regions (Cherkauer and Lettenmaier 1999). The freeze–thaw cycle would change the hydraulic conductivity of the soil significantly, resulting in a completely different environment for moisture transport within a soil column in comparison to that without considering the freeze–thaw cycle (Cherkauer and Lettenmaier 1999). Conversely, the change of soil moisture modifies the soil heat capacity and influences soil heat conductivity (Cherkauer and Lettenmaier 1999). (2) It uses a crude algorithm to model the snow dynamics based on the amount of precipitation, air temperature, and elevation (Vorosmarty et al. 1989). A proper simulation of snow thickness is

important to modeling soil thermal dynamics and hydrological dynamics, as well as ecosystem and biogeochemical dynamics, in the arctic regions (e.g. Riseborough et al. 2008). For instance, different depths of snow accumulation will start or stop the freeze–thaw cycle differently, which would further change the hydrological dynamics, particularly surface water infiltration and the water transportation in the soil profile (Cherkauer and Lettenmaier 1999; Iwata et al. 2008), and consequently change the soil thermal dynamics and ecological processes, including soil degradation, nutrient availability, and ultimately carbon dynamics.

In this study, the revised modeling framework of snow, hydrological dynamics and soil thermal dynamics is applied to two dominant ecosystem types including tundra and boreal forests in Alaska. The historical and future regional scale soil thermal and hydrological dynamics are analyzed from 1923–2099. The changes of growing season (length, onset, and ending) are then estimated based on soil thermal regimes for the same temporal and spatial domains.

2 Methods

We modify the existing framework with following aspects: (1) Incorporating a snow model that can provide reasonable daily snow depth as well as snow density, using simple formulations, while accounting for the physical processes involved as complete as possible; (2) explicitly modeling the feedbacks between soil thermal and hydrological dynamics; and (3) developing the framework at a daily time step in order to better simulate growing season changes (see appendices for detailed mathematical formulations of these new developments). Below, we first introduce how we coupled a snow model to an existing framework of soil thermal and hydrological dynamics. Second, we describe the parameterizations of the modeling framework for boreal forest and tundra ecosystems in Alaska. Third, we describe how the coupled and uncoupled versions of the modeling framework were applied to Alaska to simulate soil thermal and hydrological dynamics and changes of growing season for the study period.

2.1 Coupling soil thermal, snow and hydrological dynamics

The soil thermal and hydrological models have been developed and applied in our previous studies (Zhuang et al. 2001, 2002, 2003, 2004). In these applications, water equivalent snow depth is computed using the water balance model developed by Vorosmarty et al. (1989) at a monthly time step, and snow density is derived using the snow-classification system of Sturm et al. (1995). To improve the simulation of snow dynamics at a daily time step, we first incorporate a snow model (Vehvilainen 1992; Karvonen 2003) to the existing hydrological model to simulate the daily snow depth and snow density. This snow model was found to be able to simulate the daily snow dynamics well when it is properly parameterized (e.g. Rankinen et al. 2004).

The snow model is driven by daily air temperature and daily precipitation. The precipitation is linearly partitioned into snowfall and rainfall based on two parameters, the snowfall temperature and rainfall temperature (i.e. the first two

parameters in Table 1). When the air temperature is below (above) snowfall temperature (rainfall temperature), the precipitation is completely considered as snowfall (rainfall). Snowmelt is calculated based on the degree day factor and refreezing process is modeled based on a refreezing temperature using an exponential function. The accumulated snow is allowed to hold a certain portion of water either from rainfall or snowmelt to mimic the process of snow compacting. Snow density and depth are finally computed based on the accumulated water equivalent snow depth (see Appendix 1 for a detail description).

In our earlier version of the soil thermal model, heat capacities of different soil layers are treated as parameters for both frozen and unfrozen soils, and are determined through model calibration against observations (Zhuang et al. 2001). If freezing occurs, it assumes the whole layer is frozen completely, then the soil thermal properties are shifted from that of unfrozen soils to that of completely frozen soils, and *vice versa*. In this new development, we compute soil heat conductivities following Balland and Arp (2005).

$$K_{soil} = (K_{sat} - K_{dry}) K_e + K_{dry} \quad (1)$$

where K_e is the Kersten number, K_{sat} and K_{dry} are the heat conductivities for saturated soil and dry soil, respectively (See Appendix 2 for their definitions). The volumetric heat capacities are computed as

$$C_{vol} = \sum_i V_i C_{vol,i} \quad (2)$$

with V_i being V_{om} , V_{min} , V_{cf} , V_{air} , V_{water} and V_{ice} , which are, respectively, the volumetric fraction of soil organic matters, soil minerals, soil coarse fragments, air, liquid water and ice.

Table 1 Parameters for the tundra and boreal forest ecosystems used by the snow model in regional application

Parameter	Tundra	Boreal Forest	Unit
Temperature limit precip. falls as snow (T_{snow})	-0.55	-5.84	°C
Temperature limit precip. falls as rainfall (T_{rain})	1.20	2.72	°C
Base temperature for snowmelt ($T_{B,M}$)	0.54	3.64	°C
Min. value for degree-day factor (K_{MIN})	2.78	2.35	mm day ⁻¹ °C ⁻¹
Max. value for degree-day factor (K_{MAX})	3.25	8.26	mm day ⁻¹ °C ⁻¹
Increase in degree-day factor (K_{CUM})	0.055	0.08	mm ⁻¹
Max. retention capacity of snow ($f_{C,MAX}$)	0.21	0.28	None
Min. retention capacity of snow ($f_{C,MIN}$)	0.029	0.0	None
Decrease in retention capacity of snow (C_{CUM})	0.044	0.05	mm ⁻¹
Base temperature for refreezing ($T_{B,F}$)	-0.63	-0.98	°C
Refreezing parameter (K_F)	1.77	0.7	mm day ⁻¹ °C
Exponent for refreezing (e_F)	1.14	0.38	°C
Density of completely wet snow (ρ_{MAX})	0.36	0.3	kg dm ⁻³
Density of new snow (ρ_{NEW})	0.10	0.12	kg dm ⁻³
Daily increase in snow density due to aging (ρ_{PACK})	0.011	0.02	None

In the new framework, the fraction of liquid water of the total soil water content for each layer is determined as a function of soil temperature (See Appendix 3 for details). We still prescribe the organic matter content and the bulk density for each layer. The soil liquid water redistribution is simulated by solving the Richard's equation with top boundary condition determined by surface infiltration and evapotranspiration, and lower boundary condition by gravitational drainage (Zhuang et al. 2004). We reformulate the calculation of soil hydraulic conductivities and soil matrix potentials, following Oleson et al. (2004). An impedance factor proposed by Lundin (1990) is also introduced to reduce the hydraulic conductivity in presence of frost. Thus, the impact of active layer dynamics on liquid water transportation in the soil column is accounted implicitly. The soil hydraulic properties of the top layer (e.g. mosses for boreal forest) in the model are obtained either from literature review or calibration.

2.2 Parameterizing the modeling framework

We use site-level measurements of an old black spruce ecosystem and a tundra ecosystem to parameterize the revised modeling framework. The old black spruce site is located in the northern study area of BOREAS, near the Thompson airport, Manitoba, Canada (NSA-OBS Sellers et al. 1997; Zhuang et al. 2002; Dunn et al. 2007). Soil temperatures were measured from 1994 to 2006 at depths 5, 10, 20, 50 and 100 cm. The 13-year data from 1994 to 2006 are used in parameterization. To drive the model, daily air temperature and precipitation are obtained from the Canadian National Climate Data and Information Archive (<http://www.climate.weatheroffice.ec.gc.ca/climateData/canadae.html>). The leaf area index (LAI) required by the model are obtained from our previous study (Zhuang et al. 2007) and the MODIS15A2 product (Tian et al. 2000). The tundra site is located near the Toolik Lake area (Shaver and Jonasson 2007). Meteorological data and soil temperature at depths 5, 10, 20, 50, 100 and 150 cm have been measured at a daily time step since 2000. The 6-year data from 2001 to 2006 are used for this study. Since we have no LAI data for the tundra site, the LAI data at a similar tundra site in Barrow, Alaska, extracted from MODIS15A2 product for the year 2002, are used in the simulation.

To calibrate our modeling framework, we use a modified version of the Shuffled Complex Evolution Metropolis algorithm (SCEM-UA) (Vrugt et al. 2003) by incorporating the importance sampling technique (Shachter and Peot 1989) in the reshuffling step of the original SCEM-UA, which enables a faster convergence to the global optimal. We compute the likelihood function for a parameter set $\theta^{(t)}$ as following

$$L(\theta^{(t)}|\mathbf{y}) = \exp \left[-\frac{1}{2} \sum_{i=1}^N \left(\frac{e(\theta^{(t)})}{\sigma} \right)^2 \right] \quad (3)$$

where $e(\theta^{(t)})$ measures the distance between the model simulation and observational data \mathbf{y} . The standard deviations σ of the error distributions of the observation are assumed same for all the observations used.

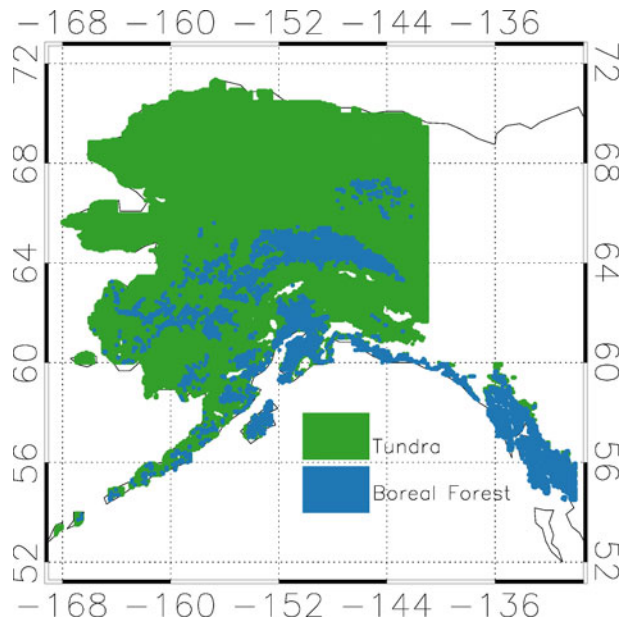
To study soil thermal dynamics in both boreal forest and tundra sites, we conduct two types of simulations: one considers the hydrological feedback on soil thermal

properties (hereinafter referred as the coupled simulation); the other has not considered the feedback of hydrological dynamics on soil thermal properties (hereinafter referred as the uncoupled simulation). For the NSA-OBS site, we use the first 3-year data from 1994 to 1997 for model calibration and the remaining for validation. For the tundra site, the first three-year data from 2001 to 2003 are used in calibration and the remaining is used in validation.

2.3 Regional simulation

We apply both the coupled and uncoupled versions of the modeling framework and the parameterizations of tundra and boreal forest ecosystems to Alaska at a $0.2^\circ \times 0.2^\circ$ (longitude by latitude) spatial resolution for the period 1923–2099 (Fig. 1). The vegetation map is re-aggregated from the $0.05^\circ \times 0.05^\circ$ resolution MODIS L3 land cover type map with the international Geosphere Biosphere Programme (IGBP) classification for year 2004 (https://lpdaac.usgs.gov/lpdaac/products/modis_products_table/land_cover/yearly_l3_global_0_05deg_cmg/mcd12c1). We re-classify the forest vegetation types as boreal forest and other types including shrub tundra, savannas, and grasslands as generic tundra. The spatially-explicit daily climate data are from the Vegetation Ecosystem Modeling and Analysis Project (Kittel et al. 2000), which was created based on the historical climate (1922–1996) and the future HadCM2 scenario (1997–2099). The soil texture and elevation are from our previous studies (Zhuang et al. 2007). We simulate the top 20 cm average soil temperature and the daily snow depths. The onset of the growing season is then defined by the date, starting from which in 10 consecutive days, the top 20 cm average

Fig. 1 Distribution of tundra and boreal forest ecosystems in Alaska for the regional application in this study, derived from the MODIS L3 land cover type map for 2004 (see text for details)



soil temperature is greater than 2°C; and the ending of growing season is defined by the date, before which, in 10 consecutive days, the top 20 cm average soil temperature is greater than 2°C. This definition should be more robust than the one defined using daily air temperature (Sharratt 1992), as our simulations indicate there are chances even when the air temperature is above zero, the top layer of a soil column is still not sufficiently thawed. We examine changes of soil thermal regime and growing season through analyses of their absolute values and anomalies at different temporal and spatial scales. The output in year 1922 is discarded in the analysis of the regional simulation because of our model configuration.

3 Results and discussion

3.1 Site-level snow dynamics

The revised modeling framework performs well at the NSA-OBS site in simulating snow depth dynamics (Fig. 2). We use 500-day data to calibrate snow model parameters (Table 1). The comparison between the simulated and observed snow thickness has a root mean square error (RMSE) 6.02 cm, coefficient of determination $R^2 = 0.90$ of the linear regression $y = 0.91x + 0.66$ ($p < 0.0001$), with x being the simulation and y being the observations. For the tundra site, we use a relatively longer time period (4-year data) in calibration. The resulting overall agreement of the simulated snow depth against the observations is of RMSE 11.47 cm, and $R^2 = 0.92$ of the linear regression $y = 0.85x + 1.03$ ($p < 0.0001$). Overall, the model captures the daily snow dynamics reasonably well.

3.2 Site-level soil thermal dynamics

For the NSA-OBS site, the simulated soil temperatures at different depths agree well with the measurements from the top soil layer to deeper soil layers (Fig. 3). The

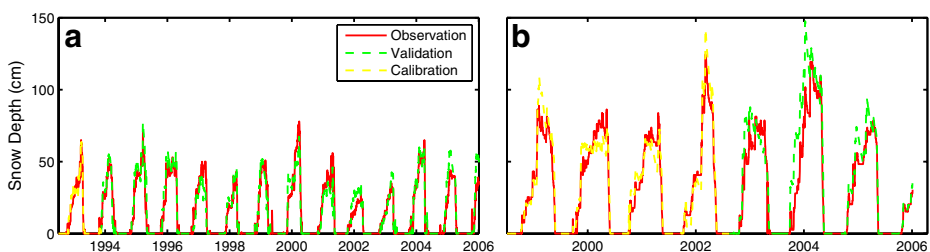


Fig. 2 Comparison of simulated snow depths versus observations. **a** NSA-OBS site: in calibration period $y = 0.970x - 0.09$ (cm), with y being the observation and x the simulation, the root mean square error (RMSE) is 3.56 (cm) and $R^2 = 0.96$ ($p < 0.0001$); in validation period $y = 0.903x + 0.75$ (cm), RMSE = 6.2 (cm) and $R^2 = 0.90$ ($p < 0.0001$). **b** Tundra site: in calibration period, $y = 0.913x + 1.40$ (cm), RMSE = 8.30 (cm), $R^2 = 0.94$ ($p < 0.0001$); in validation period $y = 0.816x + 0.17$ (cm), RMSE = 14.4 (cm), $R^2 = 0.92$ ($p < 0.0001$)

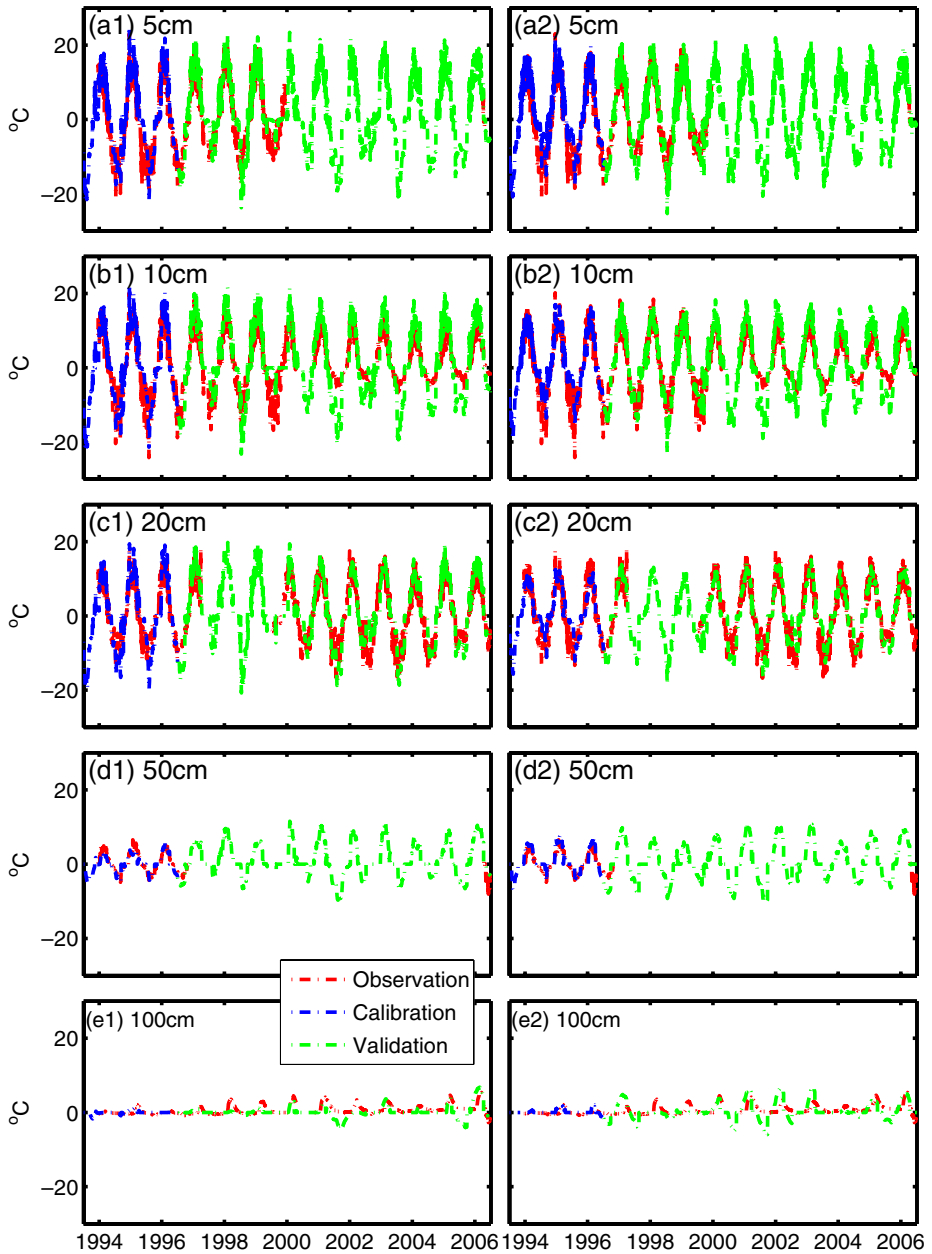


Fig. 3 Comparison between the simulated soil temperature and observations at NSA-OBS site

coupled simulation performs slightly better than the uncoupled simulation in deep soil layers (Table 2). However, as it goes deeper, the agreement becomes worse. The greater discrepancies between simulations and observations at deeper layers are mainly due to two reasons. First, in the current algorithm, only two phase planes are

Table 2 Comparison of the model simulations against the measurements in the site-level study

Depths	Tundra											
	NSA-OBS						Tundra					
	Coupled			Uncoupled			Coupled			Uncoupled		
	Slope	Int.	R ²	RMSE	Slope	Int.	R ²	RMSE	Slope	Int.	R ²	RMSE
5 cm	0.92	1.50	0.83	4.4	0.82	2.4	0.90	4.0	0.85	0.82	0.88	2.6
	1.01	0.92	0.83	4.0	1.10	-0.56	0.91	3.1	0.88	1.13	0.82	3.1
10 cm	0.98	0.42	0.83	3.9	0.77	1.35	0.88	3.4	0.86	0.92	0.83	2.7
	1.29	-0.54	0.74	5.1	1.29	-0.89	0.84	3.9	0.93	1.28	0.79	3.1
20 cm	1.07	0.03	0.81	3.9	0.68	0.97	0.80	3.5	0.81	0.85	0.77	2.7
	0.97	0.42	0.78	4.0	0.90	0.34	0.82	3.3	0.90	1.18	0.72	3.1
50 cm	0.83	-0.30	0.81	1.2	1.06	0.45	0.78	1.5	0.62	0.35	0.62	2.9
	0.60	-0.61	0.26	1.9	0.30	-1.17	0.03	3.4	0.71	0.54	0.58	2.8
100 cm	0.23	0.06	0.15	0.56	0.47	0.24	0.16	0.75	0.42	0.45	0.35	3.1
	0.57	-0.35	0.21	1.65	0.73	0.12	0.17	0.21	0.45	0.44	0.23	2.8
150 cm	NA	NA	NA	NA	NA	NA	NA	NA	0.42	0.34	0.38	2.9
	NA	NA	NA	NA	NA	NA	NA	NA	0.48	0.37	0.43	2.7

Units of slope, intercept (Int.), and root mean square error (RMSE) are N/A, °C and °C. For each different depth, the second row is statistics in the validation period

accounted explicitly in solving the heat conduction equation (Goodrich 1976). When a new phase plane is initiated at the surface in accordance with a change of freeze–thaw status, the temperature at the computational nodes (i.e. depth steps) between the new phase plane and the previous top phase plane is set to 0°C. At the next model time step, the middle phase plane is ignored and only the movements of top and bottom phase planes are tracked. This treatment appears reasonable for materials like water (see Goodrich 1976 and reference therein), but nevertheless it arbitrarily introduces or removes energy from the soil profile, resulting in solution errors. The second reason is that, we lack detailed soil moisture data to constrain the hydrological processes, and the soil profile of the black spruce forest ecosystem is approximated based on podzols (FAO-Unesco 1990). Thence there are chances that the soil moisture profile simulated deviates from the site data at a daily time step. The simulated evapotranspiration and the soil moisture in mineral layer generally agree with the observed data (Figs. 4 and 5). However, the model underestimates soil moisture in generic organic layer in year 1996 and overestimates in 1997 in comparison with the observations (Fig. 5). It is likely due to the lack of detailed information of the soil profile and sufficient soil moisture data for calibration, as we explained before.

For the tundra site, similar to the boreal forest site, the coupled simulation performs slightly better than the uncoupled simulation and greater discrepancies between the simulation and observation are found in deeper soil layers (Fig. 6, Table 2). The reasons for the deteriorating performance at deeper layers are the same as that at the boreal forest site. Also, when the linear fitting of the simulation against the measurements is conducted, the coupled version shows a slightly better performance as its slope is closer to one, and a greater R^2 value of the fitting. For instance, at depth 1.5 m, the coupled simulation has its linear fitting slope 0.42/0.48 (calibration/validation), R^2 value 0.38/0.43, and the uncoupled simulation has the slope 0.34/0.43, R^2 value 0.34/0.43.

Fig. 4 Comparison of the simulated evapotranspiration against measurement for the NSA-OBS site. In calibration period $y = 0.796x + 5.10$ (mm), RMSE = 7.51 (mm), $R^2 = 0.91$ ($p < 0.0001$); in validation period $y = 0.796x + 6.63$ (mm), RMSE = 8.89 (mm), $R^2 = 0.86$ ($p < 0.0001$)

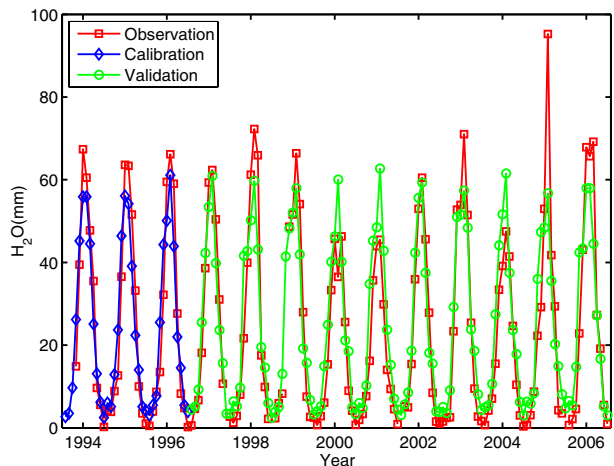
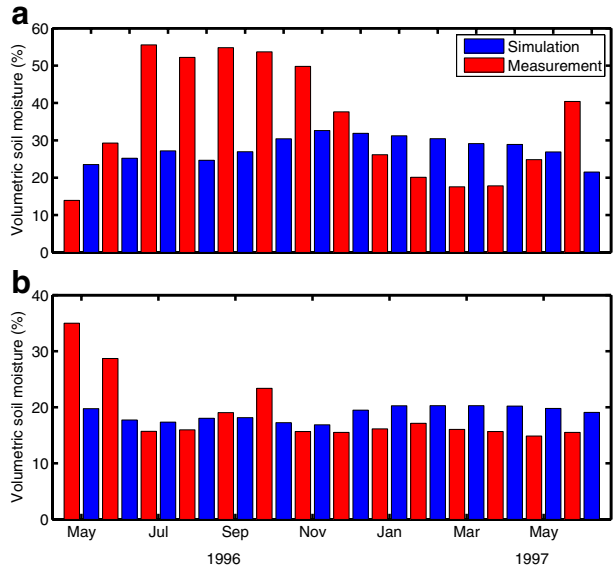


Fig. 5 Comparison between the simulated soil moisture and measurement for the for the NSA-OBS site. The temporally sporadic daily or hourly measurements of volumetric soil moisture for the humic organic and mineral soil layers are aggregated to monthly resolution for comparison. The humic organic soil moisture was estimated as the mean of all soil moisture measurements shallower than 45 cm, while the mineral soil moisture was estimated as the mean of all soil moisture measurements deeper than 45 cm and shallower than 105 cm



Through site-level studies, we obtained two sets of parameters for boreal forest and tundra ecosystems (Tables 3 and 4), which will be used for our regional extrapolation.

3.3 Historical regional soil thermal, hydrological, and growing season dynamics

3.3.1 Historical soil thermal dynamics

Soil temperature shows a significant increase over most of the study domain in response to the warming (Fig. 7). The decadal mean seasonal anomalies of the top 20 cm average soil temperature are computed for the spring (March 1st to May 31st) and autumn (September 1st to November 30th) in the 1930s, 1980s, 2030s and 2080s. The annual anomaly for a certain season in a given year is defined as the difference between the mean soil temperature for that season during the year and the mean of the mean soil temperature for that season during the period 1923–2099. The decadal mean seasonal anomaly is then calculated as the average of the annual anomalies of the season over the given decade. The computation is done separately for both the coupled and uncoupled simulations. The autumn top 20 cm mean soil temperature in the 1980s is higher than in the 1930s in most areas, in response to the increasing of air temperature, after recovering from the cold period between the 1940s and the 1970s. In the northern polar region, the autumn top 20 cm mean soil temperature in the 1980s is however lower than that in the 1930s, in accordance with the cooler autumn in the 1980s compared to the 1930s.

The soil temperature varies at different scales, and the warming trend is not very significant. In most boreal forest region (spatial anomaly not shown), the soil temperature decreases in the 1940s compared to that in the 1930s in both spring

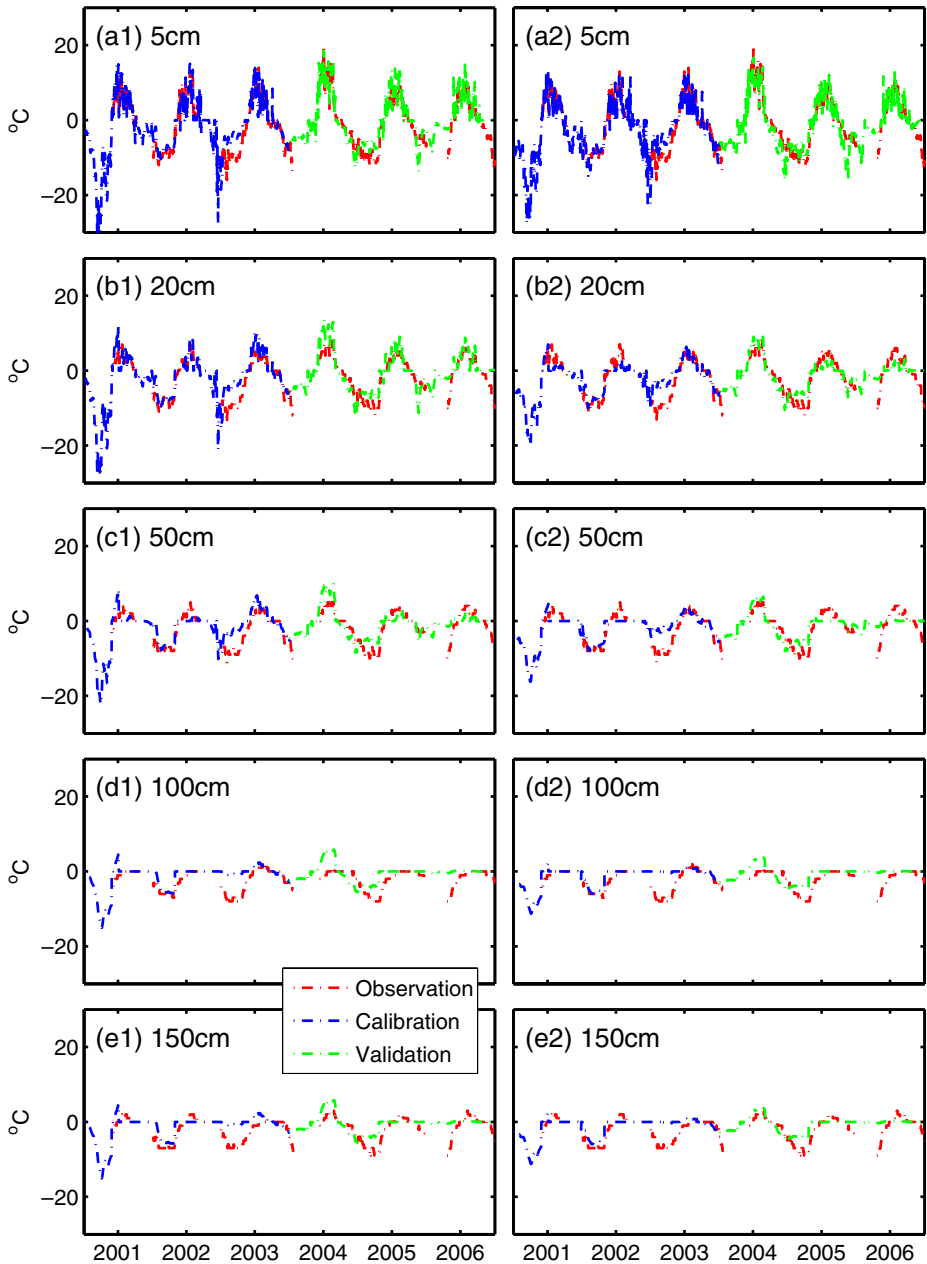


Fig. 6 Comparison between the simulated soil temperature and observations at tundra site

and autumn seasons. This decrease continues till the 1960s, and then the autumn temperature begins to increase in the 1970s, while the spring temperature still decreases. In the 1980s, the spring temperature increases almost over the whole region compared to the 1970s, and the autumn temperature increases in a smaller

Table 3 Parameters for the tundra and boreal forest ecosystems used by coupled simulation in regional application

Parameter	Tundra	Boreal Forest	Unit	Source
First layer organic matter content	90.0	71.0	%	Calibration
First layer bulk density	113.6	82.8	kg m ⁻³	Calibration
First layer saturated matric potential	-109.8	-126.8	mm	Calibration
First layer saturated hydraulic conductivity	0.15	0.12	mm ⁻¹	Calibration
First layer Clap and Hornberg constant	4.0	1.0	None	Beringer et al. (2001)
Second layer organic matter content	23.0	75.0	%	Calibration
Second layer bulk density	883.6	997.7	kg m ⁻³	Calibration
Third layer organic matter content	5.0	27.0	%	Calibration
Third layer bulk density	1043.8	1351.5	kg m ⁻³	Calibration
Fourth layer organic matter content	8.0	4.0	%	Calibration
Fourth layer bulk density	1197.0	1108.9	kg m ⁻³	Calibration
Fifth layer organic matter content	6.0	2.0	%	Calibration
Fifth layer bulk density	1123.8	1829.4	kg m ⁻³	Calibration
Sixth layer organic matter content	6.0	5.0	%	Calibration
Sixth layer bulk density	1167.0	1287.9	kg m ⁻³	Calibration

region in interior Alaska. Soil temperature in tundra ecosystems even decrease in autumn season. During the 1990s, both spring and autumn soil temperature increase at a greater rate than before.

Table 4 Parameters for the tundra and boreal forest ecosystems used by uncoupled simulation in regional application

Parameter	Tundra	Boreal Forest	Unit	Source
First layer organic matter content	85.0	94.0	%	Calibration
First layer bulk density	135.9	133.6	kg m ⁻³	Calibration
First layer volumetric water content	0.12	0.15	m ⁻³ water m ⁻³ soil	Calibration
Second layer organic matter content	23.0	74.0	%	Calibration
Second layer bulk density	855.3	979.1	kg m ⁻³	Calibration
Second layer volumetric water content	0.54	0.36	m ⁻³ water m ⁻³ soil	Calibration
Third layer organic matter content	9.0	17.0	%	Calibration
Third layer bulk density	1612.9	1040.7	kg m ⁻³	Calibration
Third layer volumetric water content	0.34	0.08	m ⁻³ water m ⁻³ soil	Calibration
Fourth layer organic matter content	4.0	4.0	%	Calibration
Fourth layer bulk density	1486.0	1148.8	kg m ⁻³	Calibration
Fourth layer volumetric water content	0.42	0.44	m ⁻³ water m ⁻³ soil	Calibration
Fifth layer organic matter content	5.0	4.0	%	Calibration
Fifth layer bulk density	1795.3	1183.7	kg m ⁻³	Calibration
Fifth layer volumetric water content	0.38	0.37	m ⁻³ water m ⁻³ soil	Calibration
Sixth layer organic matter content	7.0	4.0	%	Calibration
Sixth layer bulk density	1782.3	1462.0	kg m ⁻³	Calibration
Sixth layer volumetric water content	0.34	0.34	m ⁻³ water m ⁻³ soil	Calibration

The soil hydraulic properties of the top layer are assumed same as for the coupled simulation

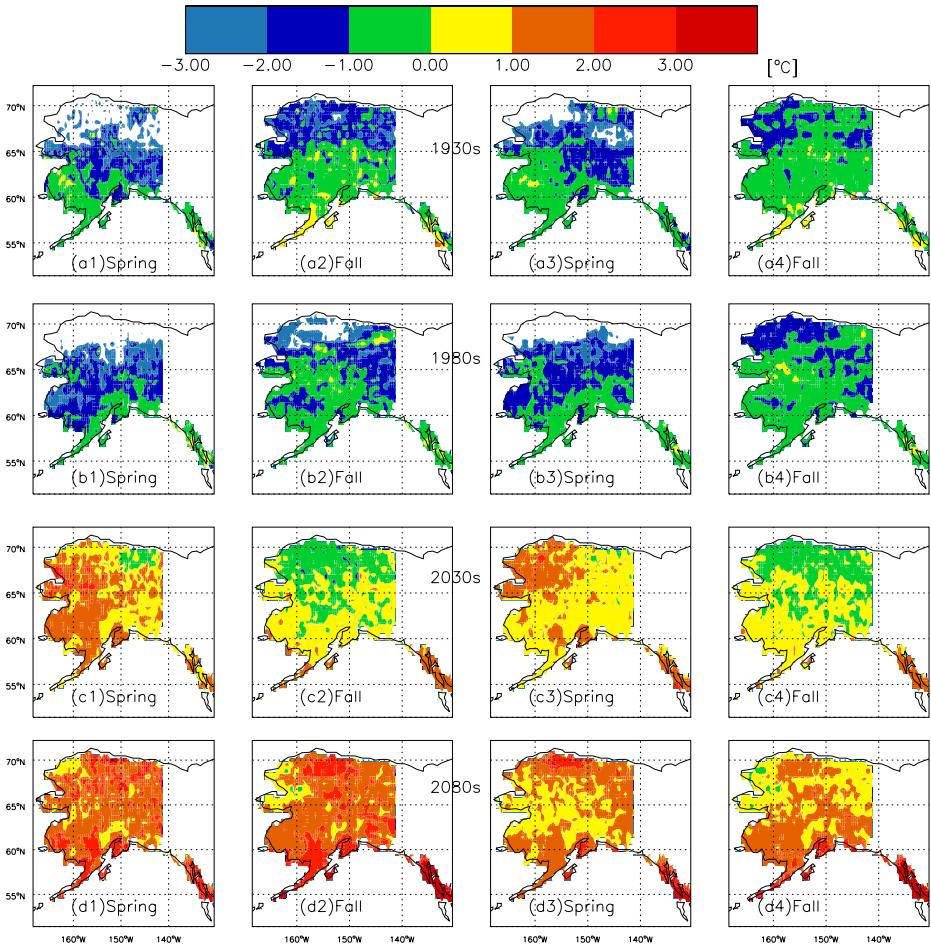


Fig. 7 Decadal anomalies of seasonal mean soil temperature of the top 20 cm soil for the four decades, separated by every 50 years. The *left two columns* are from the coupled simulation, the *right two columns* are from the uncoupled simulation

3.3.2 Historical hydrological dynamics

We define the day of last-observed snow (DLS) as the day in the first half year (DOY 1–182), after which no snow (less than 1 cm depth) is observed, the day of first-observed snow (DFS) as the day in the last half year (DOY 183–365, or DOY 183–366), before which no snow is observed, and the duration of snow-free period (DSF) as the difference between DFS and DLS.

For boreal forest ecosystems, the standard deviation of annual variation in DLS is 7.9 days in 1923–2000, and 8.1 days in 1972–2000, while for tundra ecosystems, it is 6.2 days in 1923–2000, and 5.6 days in 1972–2000 (Table 5). The variation is comparable with that in Dye (2002) (for the region 2), where the standard deviation

Table 5 Trends for snow-cover cycle variables

Analysis/region	Trend			Standard deviation		
	1923–2000	1972–2000	2010–2099	1923–2000	1972–2000	2010–2099
Boreal Forest						
Day of last observed snow	-0.9 (0.03)	-4.7 (0.01)	-2.7 (<0.01)	7.9	8.1	10.4
Day of first observed snow	-0.6 (0.03)	-1.1 (0.38)	2.0 (<0.01)	5.8	5.5	8.4
Length of snow-free period	0.2 (0.70)	3.6 (0.14)	4.7 (<0.01)	10.7	10.9	16.4
Tundra						
Day of last observed snow	-0.2 (0.48)	-2.0 (0.11)	-1.6 (<0.01)	6.2	5.6	6.3
Day of first observed snow	-0.2 (0.42)	-0.2 (0.87)	1.3 (<0.01)	4.8	5.2	5.8
Length of snow-free period	0.1 (0.96)	1.8 (0.34)	2.9 (<0.01)	8.7	8.4	10.2

Units for trends and standard deviation are, respectively, days per decade and days. Those in braces are *p* values of the linear fitting

of the week of last-observed snow cover (WLS) as he defined for the weekly, visible-band satellite observations of Northern Hemisphere snow-cover from NOAA in 1972–2000, is around 1.0 weeks (around 7.0 days). The standard deviations of the DFS and DSF of our simulated data are similar to Dye (2002)'s study. The week of first-observed snow cover (WFS) and DSF are 0.7 weeks (around 5.6 days) and 1.2 weeks (around 8.4 days), respectively, in his study. The DLS in boreal forest ecosystems and tundra ecosystems show an earlier shift of 4.7 and 2.0 days per decade, respectively. The magnitude of earlier WLS shift in Dye (2002) is 5.0 days per decade, which is greater. A possible reason is that his data are at a weekly time step, while our simulation is at a daily time step. Also, our simulation covers a smaller region than that of the region 2 in Dye (2002). For the trend in DFS, the boreal forest ecosystems and tundra ecosystems show a magnitude of -1.1 days per decade ($p = 0.38$) and -0.2 days per decade ($p = 0.87$), respectively, in 1972–2000, both of which are smaller than 0.4 days per decade in Dye (2002). The trend of our simulated DSF in boreal forest ecosystems and tundra ecosystems in 1972–2000 is 3.6 and 1.8 days per decade, still smaller than 5.3 days per decade estimated by Dye (2002). Stone et al. (2002) found the snow-melt date in northern Alaska has advanced by 8 days or so, since the mid-1960s. Our simulations show, in areas north of 69°N , that the DLS advanced 4.0 ± 2 days in the same time period. With the time series of melt dates at the Barrow (BRW) National Weather Service and NOAA/CMBDL-BRW radiometric observations and proxy estimates determined from temperature records, Stone et al. (2002) stated that the melt days have advanced by 7.7 ± 4.4 days during 1940–2000. We estimate the DLS in north of 69°N has decreased 8.7 ± 1.9 days in the same time period, which is close to their estimates. Tedesco et al. (2009) estimated, based on space-borne passive microwave data, that the snow free days have lengthened around 5 days per decade, during the period 1979–2008 for the pan arctic region. Our study indicates a trend of 1.55 days per decade ($p = 0.37$) in boreal forest ecosystems and -0.66 days per decade ($p = 0.73$) in the tundra ecosystems, which are different from Tedesco et al. (2009). This difference is mainly caused by the uncertainty in the climate data we have used, which was created before 2000 (Kittel et al. 2000).

The coupled and uncoupled simulations of soil moisture are very different at various scales (Fig. 8). Specifically, the spring volumetric soil moisture of the 1980s in the coupled simulation is relatively lower (drier) than that in the 1930s, while in the uncoupled simulation, the 1980s anomaly is higher (wetter) in most of the northern polar regions than that in the 1930s. The precipitation was generally greater in spring and summer in the 1980s than in the 1930s, and was lower in autumn in the 1980s than in the 1970s. The difference in modeled soil moisture is due to the impedance effect of the frozen water in the coupled simulation. When ice is present, the hydraulic conductivity is significantly reduced, and the amount of liquid water available for infiltration after runoff in the soil column is much less than that in the case if frozen water is otherwise neglected (Lundin 1990; Oleson et al. 2004). Therefore, in the historical period, the coupled simulation shows a different response to the variation of precipitation and evapotranspiration from the uncoupled simulation does in the region (Figs. 8 and 9). In the autumn season, the coupled simulation of soil moisture again shows a stronger positive response to the decrease of precipitation. Due to the lack of thermal impact on liquid water transport, the area-weighted moisture in the uncoupled simulation is lower than that in the coupled simulation.

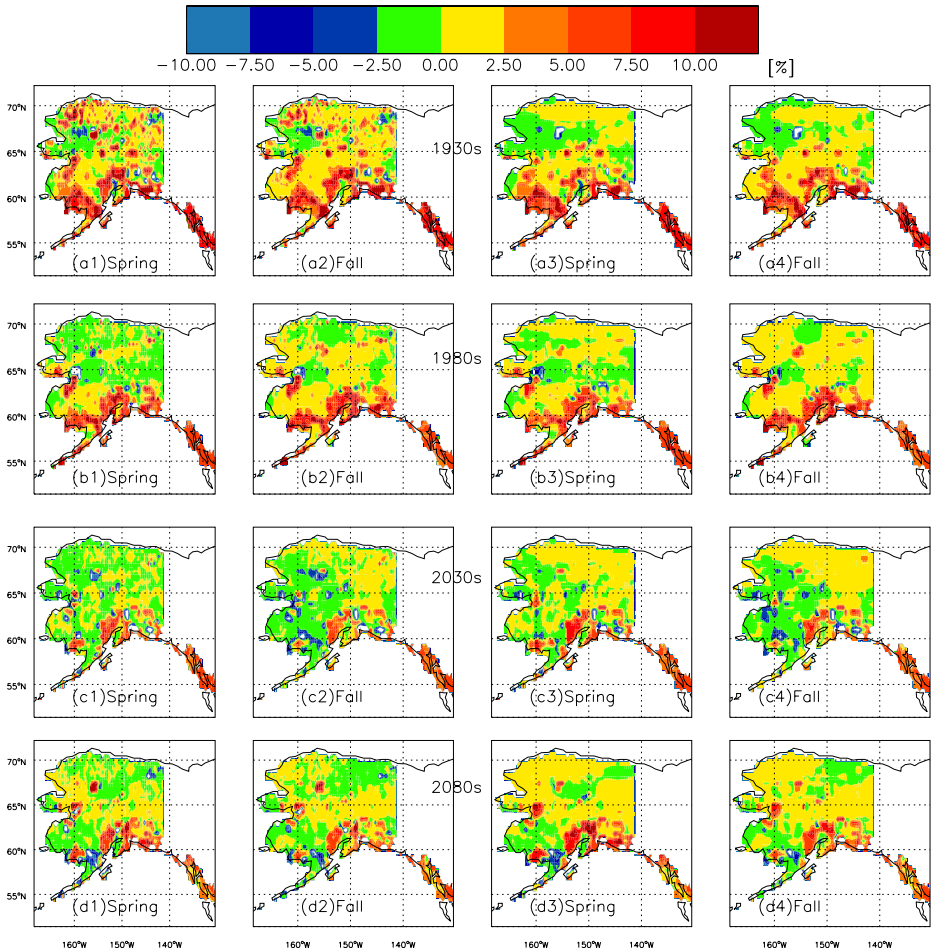
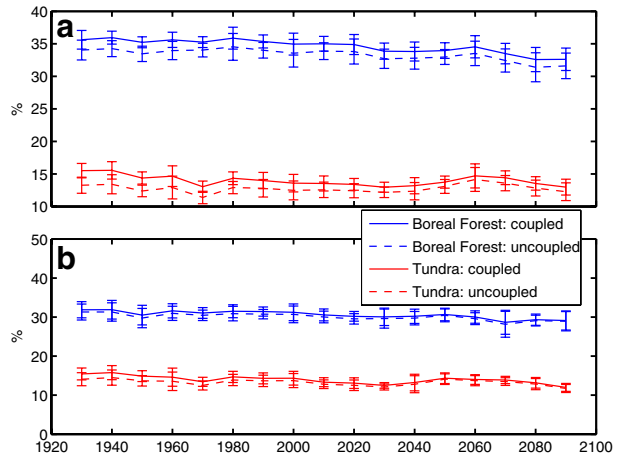


Fig. 8 Decadal anomalies of the seasonal mean organic layer soil moisture for the four decades, separated by every 50 years. The *left two columns* are from the coupled simulation, the *right two columns* are from the uncoupled simulation

3.3.3 Historical growing season changes

The area-weighted growing season lengths are estimated as 160.1 and 164.9 days in the coupled and uncoupled simulations, respectively, for the boreal forest ecosystems. For tundra ecosystems, the lengths are 118.8 and 110.27 days, respectively, in two different simulations during the period 1923–2000. The mean day of growing season onset is on the day 123.6/120.2 of the year (around May 3rd/April 30th), given in the form of coupled/uncoupled simulations (and similarly hereinafter unless explicitly stated otherwise), and ending day is 283.7/285.1 DOY (around Oct. 10th/Oct. 12th), respectively, for boreal forest ecosystems. For tundra ecosystems, the onset is 139.0/142.8 DOY (around May 18th/May 22nd) and ending day is 257.8/253.0 DOY (around Sep. 14th/Sep. 10th) respectively.

Fig. 9 Decadal area-averaged spring volumetric soil moisture of the organic layer. **a** Spring; **b** Autumn. The *error bars* show the standard deviation during the given decade



There is a strong inter-annual variability in the day of onset, day of ending and lengths of the growing seasons in our study period. Specifically, the coupled simulation shows that, for boreal forest ecosystems, in 1923, the growing season length is about 172 days; in 1924, it becomes 156 days; and in 1925, it is nearly 168 days. Similar behavior is also found for tundra ecosystems. The mean amplitudes (characterized by standard deviation) of inter-annual variation of the growing season lengths for boreal forest and tundra ecosystems are about 8.3/6.4 and 6.4/6.1 days, respectively, in the period 1923–2000. Analysis of variance shows such an inter-annual variability is almost equally contributed by the variation in the day of growing season onset and the day of growing season ending.

At a decadal scale, the growing season lengths in both boreal forest and tundra ecosystems experience a slight decrease in the 1940s and the 1950s, then an increase in the 1960s (Fig. 10). The 1960s' increasing continues to the 1990s. The changes of the growing season length can be attributed to changes in both the day of onset and the day of ending. An early day of growing season onset is not simply associated with a late day of ending. For instance, in the 1990s, when the mean growing season length is longer than that in the 1980s for boreal forest ecosystems, the mean day of onset in the 1990s is earlier than that in the 1980s, and the mean day of ending in the 1990s is later than in the 1980s. However, in the 1980s, when mean growing season length in boreal forest ecosystems is longer than that in the 1970s, both the mean day of onset and the mean day of ending are earlier than those in the 1970s.

At a longer temporal scale, the changes of growing season showed a greater variability in the historical period (Fig. 11, Table 6). During 1923–1950, the growing season lengths in tundra ecosystems in the northern polar region show a significant negative trend of change in both coupled and uncoupled simulations. The east and southwest Alaska show a lengthened growing season in the same period. When the area-averaged statistics were analyzed, both tundra and boreal forest ecosystems show the growing season lengths were shortened in 1923–1950 because of the delayed onset and advanced growing season ending. From 1950 to 2000, the area-averaged growing season length in boreal forest ecosystems increased 1.6 days per decade

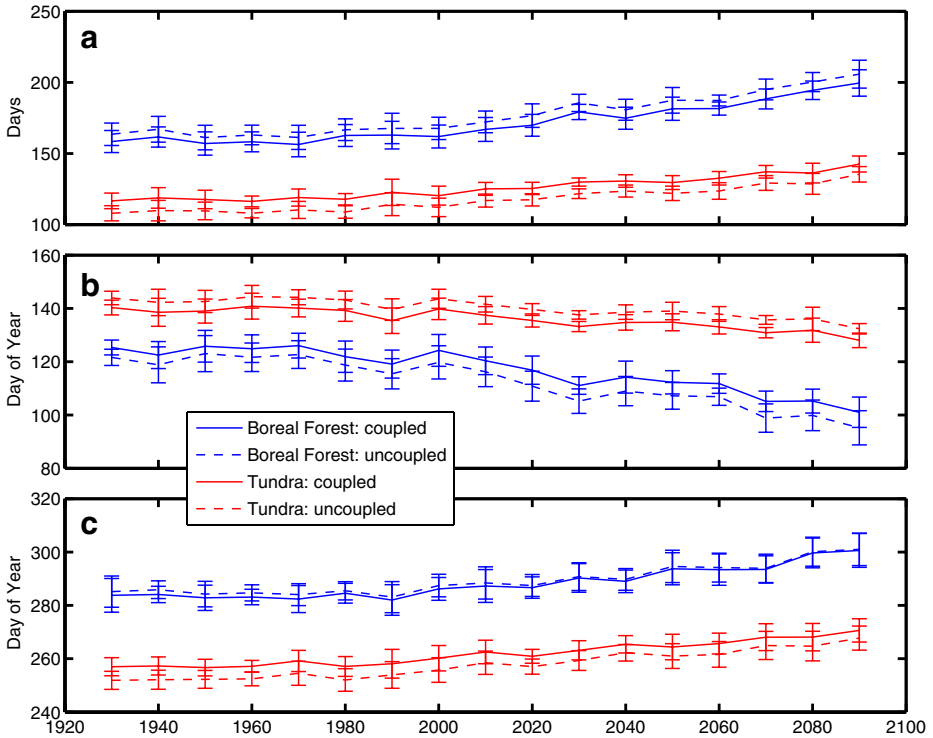


Fig. 10 **a** Decadal area-averaged growing season length. **b** Decadal area-averaged day of growing season onset. **c** Decadal area-averaged day of growing season ending. The variables are defined by days with top 20 cm soil temperature greater than 2°C, for the period 1923–2099. The error bars show the standard deviation during the given decade. See text for statistics of trend

($p = 0.05$), and 1.4 days per decade ($p = 0.02$) in tundra ecosystems in the coupled simulation. The day of onset in boreal forest ecosystems is earlier by 1.5 days per decade ($p < 0.01$) and by 0.9 days per decade ($p = 0.05$) in tundra ecosystems; the day of ending in boreal forest ecosystems is delayed by 0.1 days per decade ($p = 0.81$) and by 0.5 days per decade ($p = 0.15$) in tundra ecosystems.

Comparison between our estimates of annual growing season cycle in 1981–1990 to that derived from satellite NDVI for the region north of 45°N (Myneni et al. 1997) shows, that the day of onset was significantly shifted to an earlier DOY in both the boreal forest and the tundra ecosystems and the shift in tundra ecosystem is relatively smaller (Fig. 12). Similar to Myneni et al. (1997), we use seven successive temperature thresholds from 0.0°C (with an incremental 0.5°C) to 3.0°C to determine growing seasons and their associated variations. The area-averaged growing season onset is estimated for the coupled simulation with an advance of 13.7 ± 1.9 days (13.4 ± 2.5 days in the uncoupled simulation) for boreal forest ecosystems, and 2.2 ± 0.5 days (3.4 ± 1.2 days in the uncoupled simulation) for tundra ecosystems in the 10-year period 1981–1990 (Fig. 12). These estimates are similar to the estimate of 8 ± 3 days by Myneni et al. (1997) for the same period. For the growing season

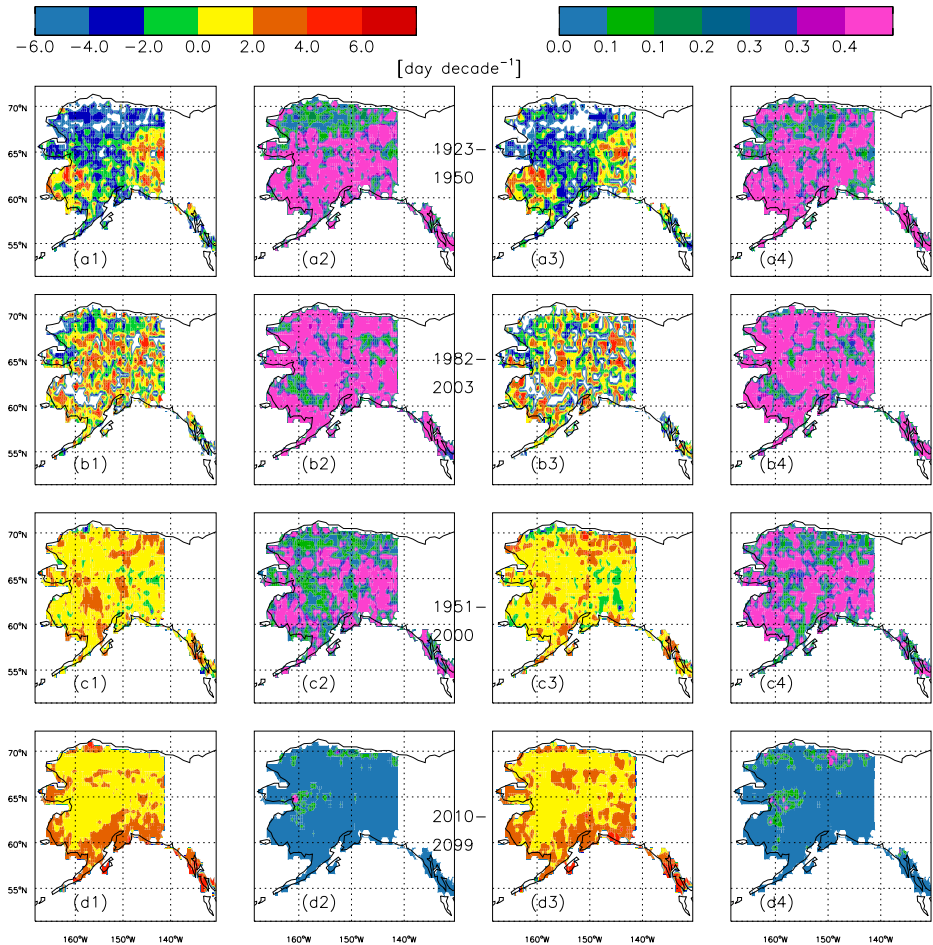


Fig. 11 Long-term trend in growing season lengths for the different time periods. The *left two columns* are for the coupled simulations, the *right two columns* are for the uncoupled simulations. *a1, a3, b1, b3, c1, c3, d1* and *d3* are the inferred trend. The rest are *p* values of the trend

ending, we estimate a delay of 3.9 ± 1.7 days (7.2 ± 3.4 days in the uncoupled simulation) and 2.5 ± 1.7 days (2.3 ± 1.4 days in the uncoupled simulation), whereas Myneni et al. (1997) estimated a prolongation of 4 ± 2 days between 1982–3 and 1989–90. We estimate that in boreal forest ecosystems the growing season length is 9.7 ± 2.8 days (6.2 ± 5.7 days in the uncoupled simulation) longer, and in tundra ecosystems 4.7 ± 2.1 days (5.7 ± 1.6 days in the uncoupled simulation) longer, which are comparable to the estimates of 12 ± 4 days longer in north of 45°N in Myneni et al. (1997) for the period 1981–1990.

Some recent studies have extended the analysis of greening and browning to the most recent periods using satellite data (Jia et al. 2003; Goetz et al. 2005; Bunn et al. 2007; Verbyla 2008). In Jia et al. (2003) and Verbyla (2008), they all found the peak NDVI increased since the 1980s, with greater increasing in the tundra ecosystems. A decreasing trend was found in boreal forest ecosystems since the 1980s

Table 6 Trend statics of the growing season onset, ending and lengths

Temporal period	1923–1950		1951–2000		2010–2099	
	Boreal Forest	Tundra	Boreal Forest	Tundra	Boreal Forest	Tundra
Coupled						
Area weighted onset	0.4 (0.71)	0.4 (0.66)	-1.5 (<0.01)	-0.9 (0.05)	-2.1 (<0.01)	-0.9 (<0.01)
Area weighted ending	-1.7 (0.18)	-0.9 (0.31)	0.1 (0.81)	0.5 (0.15)	1.7 (<0.01)	1.1 (<0.01)
Growing season length	-2.1 (0.30)	-1.3 (0.39)	1.6 (0.05)	1.4 (0.02)	3.8 (<0.01)	2.0 (<0.01)
Uncoupled						
Area weighted onset	0.9 (0.55)	0.5 (0.58)	-1.8 (<0.01)	-0.7 (0.06)	-2.2 (<0.01)	-0.9 (<0.01)
Area weighted ending	-1.5 (0.20)	-1.1 (0.23)	-0.1 (0.93)	0.6 (0.14)	1.6 (<0.01)	1.2 (<0.01)
Growing season length	-2.4 (0.29)	-1.5 (0.30)	1.7 (0.04)	1.3 (0.03)	3.8 (<0.01)	2.1 (<0.01)

Units for trends are days per decade. Those in braces are *p* values of the linear fitting

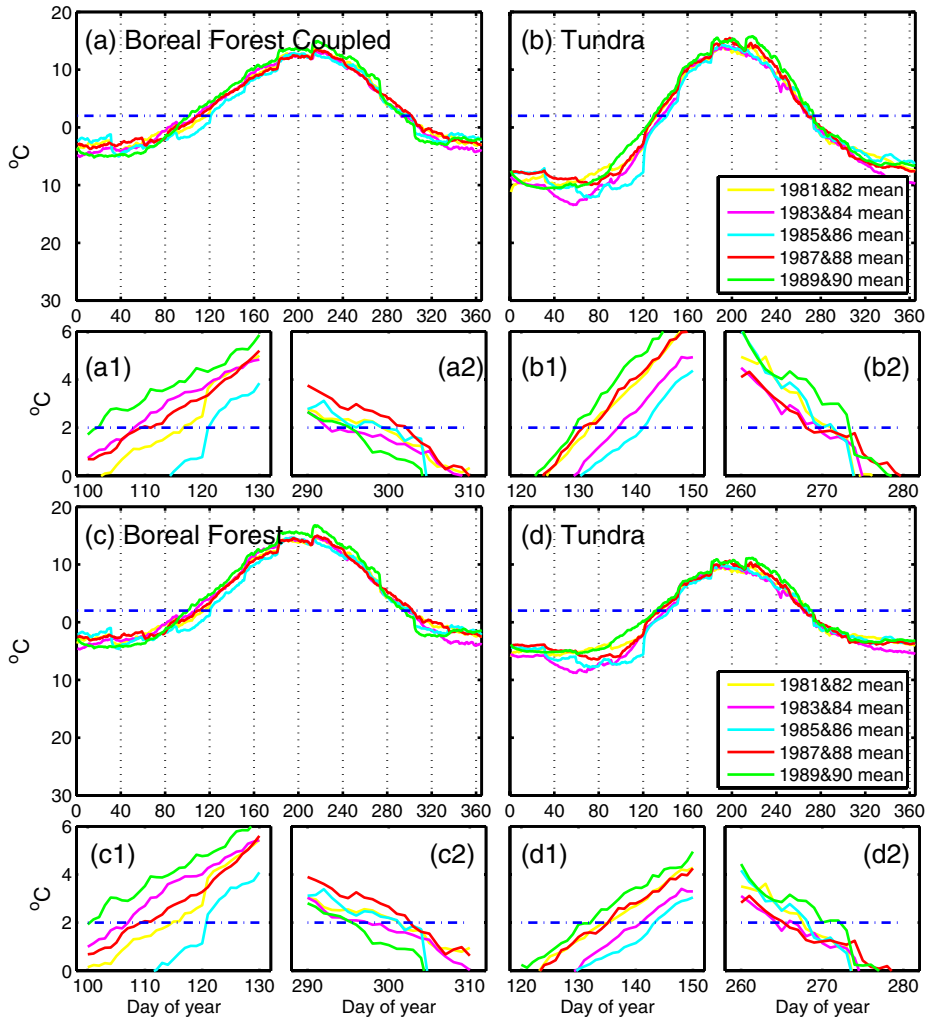


Fig. 12 Area-averaged top 20 cm soil temperature for the 1980s: (a1) and (a2), (b1) and (b2), (c1) and (c2), (d1) and (d2) are, respectively, blow-up plots for panel (a), (b), (c) and (d)

to 2000, even though with an increasing summer warmth index. The decreasing trend was explained as a result of a number of factors, including drought stress, insect and disease infestations. In our study, we found trends of increasing in growing season length are mixed with trends of decreasing throughout the Alaska (Fig. 11). Also, the soil moisture in the organic layer in the boreal forest ecosystems was found decreased both in the coupled and uncoupled simulations in the springs and autumns of this period (e.g. Fig. 9). This is in agreement with the finding of water stress in their studies. Therefore, given the climate data used in simulation, we are doing a reasonable hindcast of the soil thermal and hydrological dynamics, as

well as growing season statistics, for Alaskan terrestrial ecosystems in the historical period.

3.4 Future soil thermal and hydrological dynamics and growing season changes

Abundant inter-annual variability exists in the projected soil temperature, and the trend of soil warming is found much more significant than that in the historical period. The warming trend is found stronger in the tundra ecosystems (Fig. 7) in the northern polar region. Generally, the simulated warming in the soil thermal regime is more substantial in the coupled simulation than in the uncoupled simulation due to the modulation effects of soil moisture on soil temperature. Since the uncoupled simulation used the fixed soil moisture for each soil layer, the moisture in the second layer appears higher than that simulated in the coupled simulation. Thence the soil column in the uncoupled simulation is less sensitive to the warming because of its higher heat capacity in presence of more water.

The spring soil moisture is projected to decrease in both the coupled and uncoupled simulations because of the projected increasing in evapotranspiration (data not shown). However, as the precipitation is also projected to increase, the 2030s' mean autumn soil moisture appears higher than the 1980s' in tundra areas and the increase is found stronger in the uncoupled simulation. This is because, in the coupled simulation, the ice in tundra soils needs time to thaw in order to change the hydraulic conductivities. As warming continues, the hydraulic properties in the coupled simulation become similar to that in the uncoupled simulation, and their simulations of soil moisture become more similar (Fig. 9).

For the projected snow dynamics, the DSF in both tundra and boreal forest ecosystems increases significantly due to an earlier DLS and later DFS. From 2010 to 2099, the projected DLS approaches by 29.1 days in boreal forest ecosystems and by 23.4 days in tundra ecosystems. The projected DFS comes earlier by 12.0 days in boreal forest ecosystems and by 4.0 days in tundra ecosystems. Such changes in the DLS and DFS result in a growing season lengthening by more than 3 weeks longer by the end of the 21st century in comparison with 2010.

The mean area-weighted growing season length in 2010–2099 is 181.8/187.9 days for boreal forest ecosystems and 132.2/124.3 days for tundra ecosystems. The mean day of growing season onset and ending are 110.9/105.5 DOY, and 292.7/293.4 DOY in boreal forest ecosystems, and 133.3/137.6 DOY and 265.4/261.9 DOY in tundra ecosystems. Both boreal forest and tundra ecosystems show a significant increasing trend in the growing season length, due to an earlier onset and a later ending. The rate of growing season length increasing in boreal forest ecosystems is as much as 3.8 and 2.0 days per decade in tundra ecosystems.

We tested the sensitivity of the projection to the climate forcing by repeating the simulations by perturbing the original air temperature data $\pm 1^\circ\text{C}$ and precipitation data $\pm 10\%$. For the boreal forest ecosystem, the 1°C increase (decrease) changed the trend of DSF by 0.1 (-0.03) days per decade. The trend of DFS is more sensitive to warming than to cooling, while the opposite is for that of the DLS, but the absolute magnitude of sensitivity is less than 0.1 days per decade. For the tundra ecosystems, the 1°C increase (decrease) changed the trend of DSF by 0.02 (0.01) days per decade. Similarly, the DFS is more sensitive to warming than to cooling, while the opposite is for the DLS, with an absolute magnitude less than 0.1 days

per decade. For both the boreal forest and tundra ecosystems, the 10% increase in precipitation hardly changed the trend statistics of DLS, DFS and DSF, while the 10% decrease in precipitation changed the trend statistics of DLS, DFS and DSF by an absolute magnitude less than 0.05 days per decade. For the projection of growing season, it is found a 1°C increase (decrease) in air temperature changed the trend of growing season length by 0.04 (−0.11) days per decade for boreal forest ecosystem, and by −0.09 (0.11) days per decade for tundra ecosystem. The increase in the positive trend of growing season length in the tundra ecosystem occurred for 1°C decrease rather than for 1°C increase, is manifested as a sharper delay in the growing season ending. However, the length of growing season in the simulation with −1°C perturbation is shorter, and that with 1°C perturbation is longer. The sensitivity strengths are quite similar in both the coupled and uncoupled simulations. Similar as for the statistics of snow, the change of precipitation with ±10% did not change the statistics much (less than 0.1 days per decade in absolute magnitude) for both the boreal forest and tundra ecosystems, though the sensitivity is slightly greater in boreal forest ecosystems. Therefore, we concluded that our projection is robust with recognition of uncertainty of the forcing data used in this study.

4 Conclusions and future studies

In this study, we investigate the change of growing season through modeling soil thermal and hydrological dynamics of Alaskan tundra and boreal forest ecosystems in 1923–2099. We first revise an existing framework of soil thermal and hydrological models for the cold region by explicitly considering the interactions between soil thermal and hydrological dynamics. Our simulations suggest that the coupled version of the modeling framework performs better than the uncoupled version. The revised modeling framework well simulates soil thermal and hydrological dynamics and the changes of growing season. The estimated regional snow dynamics and growing season changes are comparable with satellite-based estimates for both tundra and boreal forest ecosystems. Our future research will incorporate the effects of fire disturbances (1) on changes of organic matter content of the top-soil layers (Lawrence et al. 2008), (2) on soil thermal conductivity and heat capacity (Zhuang et al. 2002) and (3) on hydrological dynamics in the modeling framework. We will also consider the effects of vegetation changes on snow dynamics (Arsenault and Payette 1992), thus on both soil hydrological and thermal dynamics. The new modeling framework will be further coupled with our existing biogeochemistry model, the Terrestrial Ecosystem Model (TEM; Zhuang et al. 2003, 2004, 2007) to study carbon dynamics in northern high latitudes.

Acknowledgements We thank Dr. Steve Wofsy and his group at Harvard University to make the soil temperature and latent heat flux measurements at the black spruce site available and the Ecosystem Center of Marine Biological Laboratory at Woods Hole to make the soil temperature and meteorological data at the tundra site available for this study. J. Tang is supported with the Purdue Climate Change Research Center Graduate Fellowship and NASA Earth System Science Fellowship. The research is also supported by the National Science Foundation with projects of ARC-0554811 and EAR-0630319. The computational support is from Rosen Center for High Performance Computing at Purdue University. Comments from Dr. Nigel Roulet and an anonymous reviewer and the Editor made great improvements on an earlier draft of this paper.

Appendix 1: Snow dynamics

We modify a snow model from Karvonen (2003) to compute the snow depth and density for our revised modeling framework. Given the amount of precipitation P_c (mm day⁻¹) and the corresponding air temperature T_a (°C), the amount of snowfall and rainfall is computed

$$f_W = \begin{cases} 1.0 & , \quad T_a \geq T_{rain} \\ \frac{T_a - T_{snow}}{T_{rain} - T_{snow}} & , \quad T_{snow} < T_a < T_{rain} \\ 0.0 & , \quad T_a \leq T_{snow} \end{cases} \quad (4)$$

$$P_{rain} = f_W C_W P_c$$

$$P_{snow} = (1 - f_W) C_S P_c$$

When daily air temperature T_a is below T_{snow} (°C), the precipitation falls as snow. When T_a is higher than T_{rain} (°C), the precipitation will fall as rainfall. C_W and C_S are correction factors for water and snow, whose values are, respectively, set to 1.06 and 1.32 (Karvonen 2003).

In presence of vegetation, part of the precipitation will be intercepted by plants, and the remaining falls to the ground. We following the work of Coughlan and Running (1997) to compute the snow interception by plants, such that

$$PSI = LAI \frac{I_{S,MAX}}{2}$$

$$SI_i = \min(PSI - SA_i, P_{snow,i}) \quad (5)$$

where SI_i (mm) is the snow intercepted in day i , and SA_i (mm) is the snow remains on the plants in day i after accounting for snow sublimation in the previous day. $I_{S,MAX}$ is the daily interception of snow per unit leaf area. The plant interception of rainfall is computed in a way similar to the snow interception, but the maximum intercept rate is computed using the formula in Helvey and Patric (1965).

After accounting for the plant interception, the through-fall of precipitation is added to two pools, the accumulated snow X_S (mm) and accumulated liquid water X_R (mm), on the ground, which are governed by the following equations

$$\frac{dX_S}{dt} = P_{snow,thru} - S_{melt} + S_{refreeze}$$

$$\frac{dX_R}{dt} = P_{rain,thru} - S_{refreeze} - Outflow \quad (6)$$

where $P_{snow,thru}$ (mm day⁻¹) and $P_{rain,thru}$ (mm day⁻¹) are the through-fall of snow and rain to the ground.

The snowmelt S_{melt} (mm day⁻¹) is computed based on a degree-day factor through the following equation

$$S_{melt} = K_M (T_a - T_{B,M})$$

$$K_M = K_{MIN} (1 + K_{CUM} M_{CUM}), K_M \leq K_{MAX} \quad (7)$$

where K_M is the degree-day factor (mm °C day⁻¹), $T_{B,M}$ (°C) is base temperature for melting, K_{MIN} and K_{MAX} are the minimum and maximum values for the degree-day

factor. M_{CUM} (mm) is the cumulative snowmelt during the winter/spring, and K_{CUM} (mm^{-1}) is a parameter denoting the increase in degree-day factor given one mm change in snow accumulation.

Snow is able to store a certain amount of liquid water until it becomes sufficiently “wet”, such that it reaches the maximum snow density. We model such process by introducing a water retention capacity, such that

$$f_{CAP} = f_{C,MAX}(1 - C_{CUM}M_{CUM}), f_{CAP} \geq f_{C,MIN}$$

$$S_{liq} = f_{CAP}S_{WE} \tag{8}$$

where S_{liq} (mm) is the amount of liquid water stored in the accumulated water equivalent snow S_{WE} (mm).

When temperature is low and there is liquid water stored in ground snowpack, refreezing process could occur to change liquid water into ice crystals, adding to the amount of accumulated snowpack. Such process is modeled through the following equation

$$S_{refreeze} = K_F (T_{B,F} - T_a)^{e_F}, T_a < T_{B,F}$$

$$S_{refreeze} = 0, T_a \geq T_{B,F} \tag{9}$$

where $T_{B,F}$ is the base temperature for refreezing, K_F ($\text{mm } ^\circ\text{C}^{-1} \text{ day}^{-1}$) is the refreezing parameter and e_F is the exponent coefficient for refreezing.

The outflow in day i is computed as a residual of the total liquid water X_R (mm) accumulated in day i (including new rainfall and snowmelt) after subtracting the total amount of liquid water that can be held in the wet snow (S_{liq}). If otherwise the X_R is less than S_{liq} , no outflow is allowed. The outflow, if available, is used to compute the surface runoff and infiltration following our original formulations of the model (Zhuang et al. 2004). With the amount of accumulated snowpack, the snow density and depth are computed as

$$\rho_{S,i} = \frac{(1 + \rho_{PACK})\rho_{S,i-1}D_{S,i-1} + \rho_{NEW}P_{snow,i}}{D_{S,i-1} + P_{snow,i}}$$

$$\rho_{S,i} \leq \rho_{MAX}$$

$$D_{S,i} = \frac{S_{WE,i}}{\rho_{S,i}} \tag{10}$$

where $\rho_{S,i-1}$ (kg dm^{-3}) and $D_{S,i-1}$ (mm) are snow density and snow depth of the previous day, $P_{snow,thru,i}$ is the amount of new snow through-fall in day i , ρ_{NEW} is density of new snow and ρ_{PACK} is a snow-packing parameter that accounts for the effect of snow compaction. Further, it assumes the snow density is no greater than ρ_{MAX} .

Appendix 2: Soil thermal properties

Following Balland and Arp (2005), the Kersten number is defined as, for unfrozen soils

$$K_e = \theta_{sat}^{0.5(1+V_{om,s}-\alpha V_{sand,s}-V_{cf,s})} \times \left[\left(\frac{1}{1 + \exp(-\beta\theta_{sat})} \right)^3 - \left(\frac{1 - \theta_{sat}}{2} \right)^3 \right]^{1-V_{om,s}} \tag{11}$$

and for frozen or partially frozen soils

$$K_e = \theta_{sat}^{1+V_{om,s}} \tag{12}$$

where the adjustable parameters α and β are assumed 0.24 and 18.3. V_{om} , $V_{sand,s}$ and $V_{cf,s}$ are the volumetric fractions of organic matter, sand and coarse fragments within the soil solids. θ_{sat} is the degree of saturation computed with

$$\theta_{sat} = \frac{V_{water} + V_{ice}}{V_{pores}} \tag{13}$$

where $V_{pores} = 1 - \rho_b/\rho_p$ with ρ_b being the bulk density of soil, and ρ_p the particle density of the soil, given by

$$\rho_p = W_{om}/\rho_{om} + (1 - W_{om})/\rho_{min} \tag{14}$$

where ρ_{om} and ρ_{min} are the density of soil organic matter and soil minerals, and W_{om} is the weight fraction of soil organic matter. K_{dry} and K_{sat} are, respectively, determined with

$$K_{dry} = \frac{(aK_{solid} - K_{air}) \rho_b + K_{air}\rho_p}{\rho_p - (1 - a)\rho_b} \tag{15}$$

and for saturated unfrozen soils

$$K_{sat} = K_{solid}^{1-V_{pores}} K_{water}^{V_{pores}} \tag{16}$$

and for saturated frozen soils

$$K_{sat} = K_{solid}^{1-V_{pores}} K_{ice}^{V_{pores}-V_{water}} K_{water}^{V_{water}} \tag{17}$$

K_{solid} is defined as

$$K_{solid} = K_{om}^{V_{om,s}} K_{quartz,s}^{V_{quartz,s}} K_{min}^{1-V_{om,s}-V_{quartz,s}} \tag{18}$$

Appendix 3: Water ice content formulation

We adopt the formula by Decker and Zeng (2006) to estimate the fraction of ice content in the volumetric soil moisture.

$$\frac{V_i}{V_t} = \frac{1 - \exp \left[\alpha \times \left(\frac{V_i}{V_t} \right) \times (T - T_{frz}) \right]}{\exp \left(1 - \frac{V_i}{V_t} \right)} \tag{19}$$

where V_i is volumetric ice content, V_t is total volumetric water content, and V_s is the saturated volumetric moisture content, α and β are empirical parameters, chosen 2 and 4 respectively, T_{frz} is the reference temperature for freezing.

Appendix 4: Evapotranspiration modeling

The evapotranspiration is computed as a sum of plant evapotranspiration, soil surface transpiration, plus snow sublimation from both the ground and canopy if snow is present. In this study, the plant evapotranspiration is calculated in the same way as in the work of Zhuang et al. (2004). The soil surface evapotranspiration is computed using the Penman-Monteith formula, following Shuttleworth and Wallace (1985). To ensure the mass balance of water, the dew formation is considered as the difference between the plant-intercepted rain and the plant evapotranspiration.

Appendix 5: Root distribution

The root distribution is required to model the effect of plant evapotranspiration at different depths in the soil profile. We model it as (Jackson et al. 1996):

$$r(d) = 1 - \gamma^d \quad (20)$$

where $r(d)$ is the cumulative root fraction from the soil surface to depth d (cm), and γ is the extinction coefficient derived empirically. For this study, we set γ to 0.943 for boreal forest and to 0.914 for tundra.

References

- Arsenault D, Payette S (1992) A postfire shift from lichen-spruce to lichen-tundra vegetation at tree line. *Ecology* 73(3):1067–1081
- Balland V, Arp PA (2005) Modeling soil thermal conductivities over a wide range of conditions. *J Environ Eng Sci* 4:549–558. doi:10.1139/S05-007
- Balshi MS, McGuire AD, Zhuang Q, Mellio J, Kicklighter DW, Kasichke E, Wirth C, Flannigan M, Harden J, Clein JS, Burnside TJ, McAllister J, Kurz WA, Apps M, Shvidenko A (2007) The role of historical fire disturbance in the carbon dynamics of the pan-boreal region: a process-based analysis. *J Geophys Res* 112:G02029. doi:10.1029/2006JG000380
- Beringer J, Lynch AH, Stuart CE, Mack M, Bonan GB (2001) The representation of arctic soils in the land surface model: the importance of mosses. *J Climate* 14:3324–3335
- Bunn AG, Goetz SJ, Kimball JS, Zhang K (2007) Northern high-latitude ecosystems respond to climate change. *Transactions, American Geophysical Union (EOS)* 88(34):333–335
- Cherkauer KA, Lettenmaier DP (1999) Hydrologic effects of frozen soils in the upper Mississippi river basin. *J Geophys Res* 104(D16):19599–19610
- Coughlan JC, Running SW (1997) Regional ecosystem simulation: a general model for simulating snow accumulation and melt in mountainous terrain. *Landsc Ecol* 12:119–136
- Decker M, Zeng X (2006) An empirical formulation of soil ice fraction based on in situ observations. *Geophys Res Lett* 33:L05402. doi:10.1029/2005GL024914
- Dunn AL, Barford CC, Wofsy SC, Goulden ML, Daube BC (2007) A long-term record of carbon exchange in a boreal black spruce forest: means, response to interannual variability, and decadal trends. *Glob Chang Biol* 13:577–590. doi:10.1111/j.1365-2486.2006.01221.x
- Dye DG (2002) Variability and trends in the annual snow-cover cycle in northern hemisphere land areas, 1972–2000. *Hydrol Process* 16:3065–3077. doi:10.1002/hyp.1089

- Euskirchen ES, McGuire AD, Kicklighter DW, Zhuang Q, Clein JS, Dargaville R, Dye DG, Kimball JS, McDonald KC, Mellilo JM, Romanovsky VE, Smith NV (2006) Importance of recent shifts in soil thermal dynamics on growing season length, productivity, and carbon sequestration in terrestrial high-latitude ecosystems. *Glob Chang Biol* 12:731–750. doi:[10.1111/j.1365-2486.2006.01113.x](https://doi.org/10.1111/j.1365-2486.2006.01113.x)
- FAO-Unesco (1990) Soil map of the world. Revised legend, Tech. rep., FAO, Rome, world Soil Resources. Rep. 60
- Goetz SJ, Bunn AG, Fiske GJ, Houghton RA (2005) Satellite-observed photosynthetic trends across boreal North America associated with climate and fire disturbance. *PNAS* 102(38). doi:[10.1073/pnas.0506179102](https://doi.org/10.1073/pnas.0506179102)
- Goodrich LE (1976) A numerical model for assessing the influence of snow cover on the ground thermal regime. Ph.D. thesis, McGill Univ., Montreal, Quebec
- Hansen J, Nazarenko L, Ruedy R, Sato M, Willis J, Genio AD, Kock D, Lacis A, Lo K, Novakov SMT, Perlwitz J, Russell G, Schmidt GA, Tausnev N (2005) Earth's energy imbalance: confirmation and implications. *Science* 308(5727):1431–1435. doi:[10.1126/science.1110252](https://doi.org/10.1126/science.1110252)
- Helvey JD, Patric JH (1965) Canopy and litter interception of rainfall by hardwoods of Eastern United States. *Water Resour Res* 1(2):193–206
- Iwata Y, Hayashi M, Hirota T (2008) Comparison of snowmelt infiltration under different soil-freezing conditions influenced by snow cover. *Vadose Zone J* 7:79–86. doi:[10.2136/vzj2007.0089](https://doi.org/10.2136/vzj2007.0089)
- Jackson RB, Canadell J, Ehleringer JR, Mooney HA, Sala OE, Schulze ED (1996) A global analysis of root distributions for terrestrial biomes. *Oecologia* 108:389–411
- Jia GJ, Epstein HE, Walker DA (2003) Greening of arctic Alaska, 1981–2001. *Geophys Res Lett* 30:2067. doi:[10.1029/2003GL018268](https://doi.org/10.1029/2003GL018268)
- Jones PD, New M, Parker DE, Martin S, Rigor IG (1999) Surface air temperature and its changes over the past 150 years. *Rev Geophys* 37(2):173–199
- Karvonen T (2003) Influence of global climatic change on different hydrological variables. www.water.hut.fi/wr/kurssit/Yhd-12.135/kirja/paa_e.htm
- Kimball JS, McDonald KC, Frolking S, Running SW (2004) Radar remote sensing of the spring thaw transition across a boreal landscape. *Remote Sens Env* 89:163–175
- Kimball JS, Zhao M, McGuire AD, Heinsch FA, Clein J, Calef M, Jolly WM, Kang SM, Euskirchen SE, McDonald KC, Running SW (2007) Recent climate-driven increases in vegetation productivity for the western arctic: evidence of an acceleration of the northern terrestrial carbon cycle. *Earth Interact* 11:1–30
- Kittel TGF, Rosenbloom NA, Kaufman C, Royle JA, Daly C, Fisher HH, Gibson WP, Aulenbach S, McKeown R, Schimel DS, VEMAP2 Participants (2000) VEMAP phase 2 historical and future scenario climate database. <http://www.cgd.ucar.edu/vemap>
- Lawrence DM, Slater AG, Romanovsky VE, Nicolsky DJ (2008) Sensitivity of a model projection of near-surface permafrost degradation to soil column depth and representation of soil organic matter. *J Geophys Res* 113:F02011. doi:[10.1029/2007JF000883](https://doi.org/10.1029/2007JF000883)
- Lundin L (1990) Hydraulic properties in an operational model of frozen soil. *J Hydrol* 118:289–310
- Myneni RB, Keeling CD, Tucker CJ, Asrar G, Nemani RR (1997) Increased plant growth in the northern high latitudes from 1981 to 1991. *Nature* 386:698–702
- Oleson KW, Dai Y, Bonan G, Bosilovich M, Dickinson R, Dirmeyer P, Hoffman F, Houser P, Levis S, Niu GY, Thornton P, Vertenstein M, Yang ZL, Zeng X (2004) Technical description of the community land model (CLM). nCAR/TN-461+STR
- Rankinen K, Karvonen T, Butterfield D (2004) A simple model for predicting soil temperature in snow-covered and seasonally frozen soil: model description and testing. *Hydrol Earth Syst Sci* 8(4):706–716
- Riseborough D, Shiklomanov N, Eitzelmuller B, Marchenko S (2008) Recent advances in permafrost modeling. *Permafrost Periglacial Process* 19(2):137–156. doi:[10.1002/ppp.615](https://doi.org/10.1002/ppp.615)
- Sellers PJ, Hall FG, Kelly RD, Black A, Baldocchi D, Berry J, Ryan M, Ranson KJ, Crill PM, Lettenmaier DP, Margolis H, Cihlar J, Newcomer J, Fitzjarrald D, Jarvis PG, Gower ST, Halliwell D, Williams D, Goodison B, Wickland DE, Guertin FE (1997) BOREAS in 1997: experiment overview, scientific results, and future directions. *J Geophys Res* 102(D24):28731–28769
- Serreze MC, Walsh JE, Chapin FS III, Osterkamp T, Dyurgerov M, Romanovsky V, Oechel WC, Morison J, Zhang T, Barry RG (2000) Observational evidence of recent change in the northern high-latitude environment. *Climatic Change* 46:159–207
- Shachter RD, Peot MA (1989) Simulation approaches to general probabilistic inference on belief networks. In: *Uncertainty in artificial intelligence*, vol 5. Elsevier Science Publishing Company, Inc, New York, NY, pp. 221–231

- Sharratt BS (1992) Growing season trends in the Alaskan climate record. *Arctic* 45(2):124–127
- Shaver GR, Jonasson S (2007) Response of Arctic ecosystems to climate change: result of long-term field experiments in Sweden and Alaska. *Polar Res* 18(2):245–252
- Shuttleworth WJ, Wallace JS (1985) Evaporation from sparse crops—an energy combination theory. *Q J Royal Meteorol Soc* 111:839–855
- Slayback DA, Pinzon JE, Los OS, Tucker CJ (2003) Northern hemisphere photosynthesis trends 1982–1999. *Glob Chang Biol* 9:1–15
- Stone RS, Dutton EG, Harris JM, Longenecker D (2002) Earlier spring snowmelt in northern Alaska as an indicator of climate change. *J Geophys Res* 107(D10):4089. doi:[10.1029/2000JD000286](https://doi.org/10.1029/2000JD000286)
- Sturm M, Holmgren J, Liston GE (1995) A seasonal snow cover classification system for local to global applications. *J Clim* 8(5):1261–1283
- Tedesco M, Brodzik M, Armstrong R, Savoie M, Ramage J (2009) Pan arctic terrestrial snowmelt trends (1979–2008) from space-borne passive microwave data and correlation with the Arctic Oscillation. *Geophys Res Lett* 36:L21402. doi:[10.1029/2009GL039672](https://doi.org/10.1029/2009GL039672)
- Tian Y, Zhang Y, Knyazikhin Y, Myneni RB, Running SW (2000) Prototyping of MODIS LAI/FPAR algorithm with LASUR and landsat data. *IEEE Trans GeoSci Remote Sens* 38(5):2387–2401
- Vehvilainen B (1992) Snow cover models in operational watershed forecasting, National Board of Waters and the Environmental, Finland. Publications of Water and Environmental Research Institute, 112 pp
- Verbyla B (2008) The greening and browning of Alaska based on 1982–2003 satellite data. *Glob Ecol Biogeogr* 17:547–555. doi:[10.1111/j.1466-8238.2008.00396.x](https://doi.org/10.1111/j.1466-8238.2008.00396.x)
- Vorosmarty CJ, Peterson BJ, Rastetter EB, Steudler PA (1989) Continental scale models of water balance and fluvial transport: an application to South America. *Glob Biogeochem Cycles* 3(3):241–265
- Vrugt JA, Gupta HV, Bouten W, Sorooshian S (2003) A shuffled complex evolution metropolis algorithm for optimization and uncertainty assessment of hydrological model parameters. *Water Resour Res* 39:8. doi:[10.1029/2002WR001642](https://doi.org/10.1029/2002WR001642)
- Zhuang Q, Romanovsky VE, McGuire AD (2001) Incorporation of a permafrost model into a large-scale ecosystem model: evaluation of temporal and spatial scaling issues in simulating soil thermal dynamics. *J Geophys Res* 106:33649–33670. doi:[10.1029/2001JD900151](https://doi.org/10.1029/2001JD900151)
- Zhuang Q, McGuire AD, O'Neill KP, Harden JW, Romanovsky VE, Yarie J (2002) Modeling soil thermal and carbon dynamics of a fire chronosequence in interior Alaska. *J Geophys Res* 108(D1):8147. doi:[10.1029/2001JD001244](https://doi.org/10.1029/2001JD001244)
- Zhuang Q, McGuire AD, Mellilo JM, Clein JS, Dargaville RJ, Kicklighter DW, Myneni RB, Dong J, Romanovsky VE, Harden J, Hobbie JE (2003) Carbon cycling in extratropical terrestrial ecosystems of the northern hemisphere during the 20th century: a modeling analysis of the influences of soil thermal dynamics. *Tellus* 55B:751–776
- Zhuang Q, Mellilo JM, Kicklighter DW, Prinn RG, McGuire AD, Steudler PA, Felzer BS, Hu S (2004) Methane fluxes between terrestrial ecosystems and the atmosphere at northern high latitudes during the past century: a retrospective analysis with a process-based biogeochemistry model. *Glob Biogeochem Cycles* 18:GB3010. doi:[10.1029/2004GB002239](https://doi.org/10.1029/2004GB002239)
- Zhuang Q, Melillo JM, McGuire AD, Kicklighter DW, Prinn RG, Steudler PA, Felzer RS, Hu S (2007) Net emissions of CH₄ and CO₂ in Alaska: implications for the region's greenhouse gas budget. *Ecol Apps* 17(1):203–212
- Zimov SA, Schuur EAG, Chapin FS III (2006) Climate change: permafrost and the global carbon budget. *Science* 312(5780):1612–1613. doi:[10.1126/science.1128908](https://doi.org/10.1126/science.1128908)